Sir-two-homolog 2 (Sirt2) modulates peripheral myelination through polarity protein Par-3/atypical protein kinase C (aPKC) signaling

Bogdan Beirowski[a], Jason Gustin[b], Sean M. Armour[c], Hiroyasu Yamamoto[d], Andreu Viader[a], Brian J. North[c], Shaday Michán[e], Robert H. Baloh[f,g], Judy P. Golden[h], Robert E. Schmidt[g,i], David A. Sinclair[c], Johan Auwerx[d], and Jeffrey Milbrandt[a,g,1]

Departments of [a]Genetics, [f]Neurology, and [i]Pathology, Washington University School of Medicine, St. Louis, MO 63110; [b]Sigma–Aldrich Biotechnology, St. Louis, MO 63103; [c]Department of Pathology, Harvard University School of Medicine, Cambridge, MA 02115; [d]Laboratory for Integrative and Systems Physiology, Ecole Polytechnique Fédérale de Lausanne, 1015 Lausanne, Switzerland; [e]Instituto de Geriatria, Institutos Nacionales de Salud, Mexico D.F., 04510, Mexico; [g]Hope Center for Neurological Diseases, St. Louis, MO 63110; and [h]Department of Anesthesiology, Washington University Pain Center, St. Louis, MO 63110

Edited by Richard L. Huganir, Johns Hopkins University School of Medicine, Baltimore, MD, and approved September 7, 2011 (received for review April 11, 2011)

The formation of myelin by Schwann cells (SCs) occurs via a series of orchestrated molecular events. We previously used global expression profiling to examine peripheral nerve myelination and identified the NAD$^+$-dependent deacetylase Sir-two-homolog 2 (Sirt2) as a protein likely to be involved in myelination. Here, we show that Sirt2 expression in SCs is correlated with that of structural myelin components during both developmental myelination and remyelination after nerve injury. Transgenic mice lacking or overexpressing Sirt2 specifically in SCs show delays in myelin formation. In SCs, we found that Sirt2 deacetylates Par-3, a master regulator of cell polarity. The deacetylation of Par-3 by Sirt2 decreases the activity of the polarity complex signaling component aPKC, thereby regulating myelin formation. These results demonstrate that Sirt2 controls an essential polarity pathway in SCs during myelin assembly and provide insights into the association between intracellular metabolism and SC plasticity.

neuropathy | sirtuin | acetylation

Myelinating Schwann cells (SCs) perform a range of tasks required for correct function of the peripheral nervous system (PNS). In addition to ensuring normal locomotion and sensation and providing trophic support of axons (1), they control regenerative and reparative responses in peripheral nerves (2). These functions are tightly linked to the ability of differentiated SCs to intimately associate with axons and ensheath them with compact myelin. Various pathways in SCs have been identified that are crucial for this process including neuronal growth factors, cell adhesion, and a number of second messenger systems (3). These pathways are interrelated with strict temporal control of key transcription factors, collectively responsible for up-regulation of genes critical for structural assembly of myelin (3, 4).

Metabolic derangements contribute to a major class of conditions in which SC function is impaired. For example, numerous studies indicate that nerve regeneration and myelination after injury are impaired in diabetic neuropathy (5–8). Moreover, SC myelination can be altered by changes in nutrition (9, 10). These findings give rise to the idea that abnormal metabolic conditions could lead to aberrant myelination via abnormalities in SC function. We previously identified Sir-two-homolog 2 (Sirt2) in gene expression profiling experiments as a putative myelination-associated protein on the basis of the similarity of its expression to that of mRNAs encoding structural myelin proteins during periods of myelin formation (11). Sirt2 is a member of the conserved sirtuin family of NAD$^+$-dependent deacetylases that modulate cellular processes in accord with the metabolic state (12, 13). Depending on the cellular context and tissue type, Sirt2 is reported to deacetylate α-tubulin (14, 15), control cell division (16), regulate adipocyte differentiation through FOXO1 (17), and alter gene expression via the deacetylation of histone H4 (18) among other functions.

Here, we demonstrate that normal elaboration of peripheral myelin by SCs requires regimented temporal expression of Sirt2. This expression, in turn, ensures proper temporal regulation of Par-3 acetylation and activation of the polarity signaling component atypical protein kinase C (aPKC) during the myelination program. Building on the discovery of Sirt2 interactions with the polarity complex, newly generated Sirt2 mouse mutants, and the study of in vivo and in vitro myelination paradigms, our data indicate that Sirt2 modulates SC peripheral myelination. These findings extend our understanding of the molecular mechanisms underlying metabolic effects on myelination and hence the impaired SC plasticity observed in diseases, like diabetes, that are characterized by abnormal metabolism and peripheral neuropathy.

Results

Induction of Sirt2 Expression in SCs Is Correlated with Peripheral Myelination. To gain insight into the myelination process, we previously performed gene expression profiling in sciatic nerves during nerve development and during remyelination after nerve injury (11). During this analysis, we identified Sirt2 as a gene that was coexpressed with myelin structural proteins in peripheral nerves, thus implicating it as a potential regulator of myelination. In line with data from other cells (14), fluorescence immunostaining in primary SC cultures demonstrated clear cytoplasmic localization of Sirt2 (Fig. 1*A*). Teased fiber preparations showed prominent Sirt2 staining in perinuclear SC areas, paranodal SC regions directly flanking the node that is demarcated by Na_V staining, and along internodes associated with E-cadherin labeling (Fig. 1 *B–D*). This result indicates that Sirt2 is abundant in areas of noncompact myelin, such as paranodal loops and Schmidt–Lanterman (SL) incisures.

To investigate coregulation of Sirt2 with integral myelin proteins during peripheral myelin formation, we compared their re-

Author contributions: B.B., J.G., S.M.A., H.Y., A.V., B.J.N., and J.M. designed research; B.B., J.G., S.M.A., H.Y., A.V., B.J.N., S.M., and J.P.G. performed research; S.M., R.H.B., R.E.S., D.A.S., and J.A. contributed new reagents/analytic tools; B.B., J.G., S.M.A., H.Y., A.V., B.J.N., and J.P.G. analyzed data; and B.B. and J.M. wrote the paper.

Conflict of interest statement: The authors and Washington University may derive benefit from a licensing agreement with Sirtris Pharmaceuticals, which did not provide any support for this work.

This article is a PNAS Direct Submission.

[1]To whom correspondence should be addressed. E-mail: JMilbrandt@WUSTL.EDU.

See Author Summary on page 17593.

This article contains supporting information online at www.pnas.org/lookup/suppl/doi:10.1073/pnas.1104969108/-/DCSupplemental.

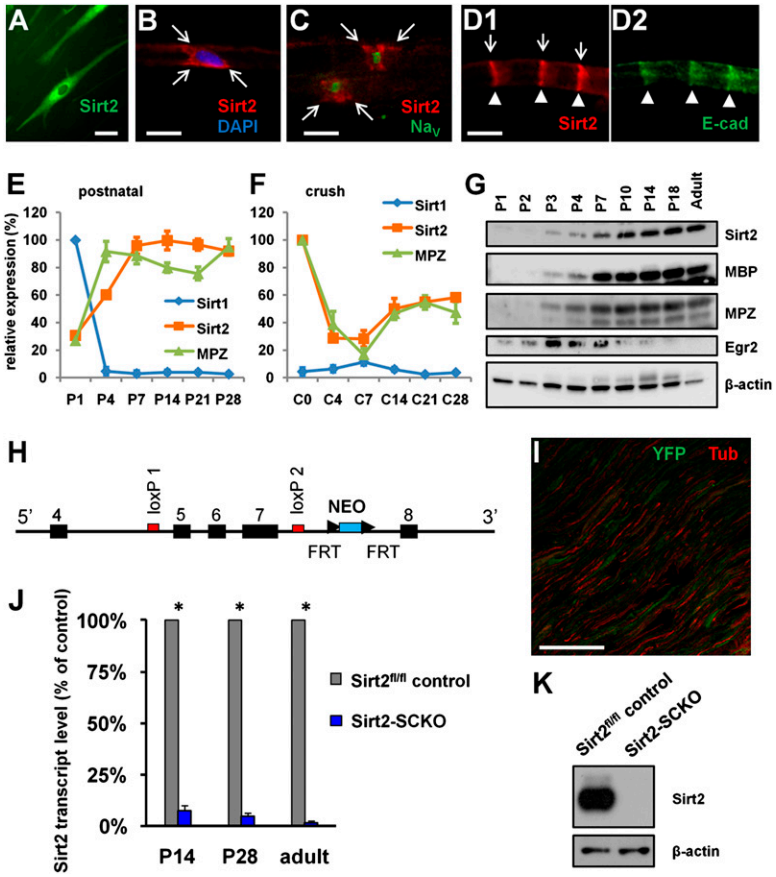

Fig. 1. Dynamic expression of Sirt2 in SCs and generation of Sirt2-SCKO mice. (*A*) Representative fluorescence microscopy of immunostained rat Schwann cell in vitro showing cytoplasmic localization of Sirt2 (green). (Scale bar: 10 μm.) (*B–D*) Fluorescence microscopy of rat teased fiber preparations following immunolabeling with antibodies against Sirt2 (red), E-cadherin (E-cad) (green), and Na_V sodium channel (green). Arrows point to Sirt2 signal. Note detection of Sirt2 in regions of noncompact myelin and colocalization of Sirt2 (*D1*) and E-cadherin (*D2*) at Schmidt–Lanterman incisures (arrowheads). (Scale bars: 2 μm.) (*E* and *F*) Graphs showing relative Sirt1, Sirt2, and MPZ mRNA levels (normalized to GAPDH expression) in mouse postnatal nerves (*E*) and distal nerve stumps at the indicated times (days) after crush injury (*F*) (n = 9 mice for each group tested). (*G*) Western blots from sciatic nerve extracts from postnatal and adult mouse probed with antibodies against Sirt2, MBP, MPZ, Egr2, and β-actin (loading control). (*H*) Schematic illustration of the conditional *Sirt2* allele with loxP sequences (red) flanking exons 5–7 (black). The neomycin selection marker cassette (NEO, blue) is flanked by Flp recombinase recognition sequences (FRT sites). (*I*) Longitudinal sciatic nerve section from mouse carrying the $Sirt2^{flox}$ and *ROSA26-YFP* alleles and expressing Cre recombinase under control of the MPZ promoter. The section was immunolabeled with anti-βIIItubulin antibody (red) to visualize axons apposed to the YFP signal derived from the ROSA allele after activation in SCs by Cre recombinase expression (green). (Scale bar: 50 μm.) (*J*) qRT-PCR quantification of relative Sirt2 transcript levels (normalized to GAPDH expression) in sciatic nerves from Sirt2-SCKO mutants and $Sirt2^{fl/fl}$ control mice without Cre recombinase expression (n = 3 mice per group tested) (*$P < 0.01$). (*K*) Western blot from sciatic nerve lysates of 2-wk-old $Sirt2^{fl/fl}$ control and Sirt2-SCKO mice probed with antibodies against Sirt2 and β-actin (loading control).

spective expression profiles. First, using qRT-PCR, the expression of Sirt2 in mouse sciatic nerve was examined during developmental myelination and remyelination after nerve injury. Strikingly, Sirt2 mRNA levels markedly increased in postnatal sciatic nerve from postnatal day P1 to P14, similar to myelin protein zero (MPZ) mRNA levels, a major myelin component (Fig. 1*E*). Thus, the induction of Sirt2 expression parallels peripheral myelination in mice. In contrast, the expression of the related sirtuin gene, Sirt1, decreased rapidly and remained low. Moreover, immediately following nerve crush injury, Sirt2 expression decreased as SCs dedifferentiate during Wallerian degeneration, but its expression increased again 7 d after injury as axonal regeneration and remyelination ensued (Fig. 1*F*). In this paradigm, Sirt2 expression again correlated with that of MPZ. In accord with Sirt2 mRNA levels, the amount of Sirt2 protein levels in sciatic nerve increased substantially between P1 and P14 and remained high into adulthood, similar to the profile of MPZ and myelin basic protein (MBP), another myelin structural component (Fig. 1*G*). Thus, the Sirt2 temporal expression pattern in SCs of the peripheral nerve is concordant with those of typical myelination proteins and lags behind that of Egr2 (Fig. 1*G*), a transcription factor that largely controls the progression from the promyelinating to the myelinating state of the SC.

Schwann Cell-Specific Ablation of Sirt2 in Mice. The dynamic Sirt2 expression led us to hypothesize that Sirt2 deacetylase activity plays a regulatory role in myelination and caused us to explore the consequences of Sirt2 ablation in SCs in vivo. For this purpose we generated a conditional $Sirt2^{flox}$ allele in which two *loxP* sites flank three critical exons (Fig. 1*H*), so that Cre recombinase-mediated excision creates a nonfunctional allele. Mice homozygous for the $Sirt2^{flox}$ allele appeared normal and were fertile. To ensure SC-specific Sirt2 ablation (Sirt2-SCKO) from early embryonic ages, $Sirt2^{flox}$ mice were crossed to MPZ-Cre mice that express Cre recombinase in SCs starting from embryonic day 14.5 (E14.5) to E15.5 (19). Sirt2-SCKO mice were born at normal Mendelian ratios and survived into adulthood despite the abnormalities described below. In a subset of these conditional knockout animals the $Sirt2^{flox}$ allele was combined with the *ROSA26-YFP* reporter allele to directly visualize Cre recombinase activity. Sciatic nerve

sections from these animals revealed YFP fluorescence in elongated cells apposed to axons, the typical morphology of SCs (Fig. 1*I*). As further confirmation of Sirt2 deletion, qRT-PCR and Western blotting demonstrated strong reduction of Sirt2 mRNA and protein levels in sciatic nerve preparations from Sirt2-SCKO mice (Fig. 1 *J* and *K*). Given that nerves also contain nonglial cells, in which recombination is not expected, these reductions reflect highly efficient ablation of Sirt2 in SCs.

Sirt2-SCKO Mice Show Transiently Delayed Myelination. To explore deficits in developmental myelination, we analyzed peripheral nerves from early postnatal Sirt2-SCKO mice and littermate controls carrying the *Sirt2*^{flox} allele but lacking the MPZ-Cre transgene. In rodents, SCs first adopt a 1:1 relationship with large-caliber axons destined to be myelinated, and nerve myelination is largely completed within 2 wk after birth. Inspection of toluidine-blue–stained sections as well as electron microscopic analysis revealed that P1, -3, and -5 sciatic nerves of Sirt2-SCKO mice were hypomyelinated (Fig. 2*A* and Fig. S1*A*). At these ages control nerves contained many thinly myelinated axons, whereas Sirt2 mutants had large clusters of densely packed axons that were completely devoid of compact myelin. The number of myelinated axon profiles per nerve section was significantly reduced in Sirt2-SCKOs at each of these ages (Fig. 2*B*). Ultrastructural analysis at higher magnification showed that many Sirt2-deficient SCs engaged in a 1:1 relationship with individual axons but failed to elaborate myelin (Fig. S1*B*). This result suggests that radial axonal sorting is normal but spiral enwrapping of axons with compact myelin is aberrant. Further analysis using quantitative histomorphometry of sciatic nerves revealed significantly higher overall *g*-ratios in P1–P5 Sirt2-SCKOs (Fig. 2*C*). This indicates that even those fibers that are myelinated in Sirt2-SCKO nerves have thinner myelin sheaths. These abnormalities were accompanied by no significant change in the number of SC nuclei per nerve section (Fig. S1*C*). Strikingly, the hypomyelination of Sirt2-SCKO nerves gradually became less pronounced (Fig. S1*A*), so that no statistically significant differences in cumulative fiber structure parameters could be detected after P7 (Fig. 2 *B* and *C*). Although no morphological abnormalities could be detected at these ages on transverse nerve sections, electrophysiological analysis revealed significantly reduced motor nerve conduction velocity in Sirt2-SCKO mice at P21 and P28, the earliest time points we were able to perform adequate measurements (Fig. S2). We searched for abnormalities in the organization of the nodal apparatus and paranodal loops that might account for the deficits in saltatory conduction in these mice, but no derangements were detected (Fig. S3 *A* and *B*). However, we did observe extensive outfoldings in compact myelin located in close vicinity to the paranode in Sirt2-SCKO mice at P21 and P28 (Fig. S3*C*). In view of the importance of properly structured internodes for nerve impulse propagation, this defect is consistent with the reduced nerve conduction velocity.

The morphological and electrophysiological impairments observed in young Sirt2-SCKO mice dissipated with age such that no abnormalities were observed in 2- to 4-mo-old animals ($n = 67$). Furthermore, several sensorimotor tests including the accelerated rotarod test, grip strength, and heat sensitivity revealed no deficits in this cohort (Fig. S4 *A*–*C*). Importantly, the improvements of morphological and electrophysiological abnormalities were not the result of an expansion of SCs that failed to excise Sirt2, because low levels of sciatic nerve Sirt2 mRNA and protein were maintained into adulthood (Fig. 1*J* and Fig. S4*D*). We conclude that Sirt2-SCKO mice show a transient delay in developmental myelination, predominantly during the phase in which Sirt2 expression levels increase most markedly in wild-type animals (Fig. 1*E*).

To examine myelination in adulthood, we used a sciatic nerve crush model in which the damaged axons regenerate and become

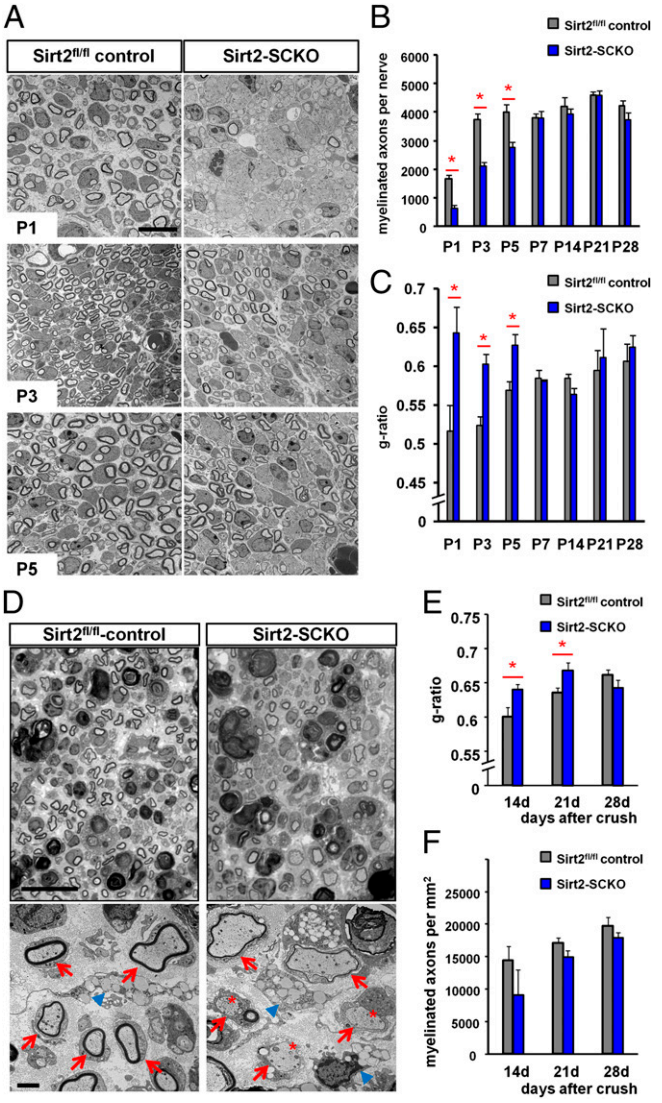

Fig. 2. Sirt2-SCKO mice display hypomyelination. (*A*) Representative electron micrographs from transverse sciatic nerve ultrathin section from Sirt2-SCKO mutants and Sirt2$^{fl/fl}$ control mice at postnatal ages P1, P3, and P5. Note reduction in the number of myelinated fibers in Sirt2-SCKO preparations. (Scale bar: 10 μm.) (*B* and *C*) Histomorphometric quantification of myelinated fiber numbers (*B*) and *g*-ratios (*C*) in transverse sciatic nerve sections from Sirt2-SCKO mutants and Sirt2$^{fl/fl}$ control mice at postnatal ages P1–P28 ($n = 3$–5 mice per group tested) (*$P < 0.05$). (*D*) Representative light (*Upper*) and electron (*Lower*) microscopy of distal sciatic nerve stumps 14 d after nerve crush injury. Red arrows point to regenerated fibers. Note thinner myelin sheaths or complete absence of compact myelin (asterisks) in axons from adult Sirt2-SCKO mice compared with Sirt2$^{fl/fl}$ controls. Blue arrowheads point to macrophages with typical cytoplasmic vacuolation due to phagocytosis. [Scale bars: 20 μm (light microscopy) and 2 μm (electron microscopy).] (*E* and *F*) Quantification of *g*-ratios (*E*) and fiber numbers (*F*) in distal sciatic nerve stumps at different time points after nerve crush injury in Sirt2-SCKO mice and Sirt2$^{fl/fl}$ controls ($n = 7$–8 mice per group tested) (*$P < 0.05$).

remyelinated (20, 21). We assessed the efficiency of remyelination by an established nerve histomorphometry method (22). Fourteen days following nerve crush, Sirt2-SCKO mice showed thinner myelin with significantly increased cumulative *g*-ratios ($P < 0.05$) (Fig. 2 *D* and *E*), indicative of reduced myelination. Electron microscopy revealed many extremely thinly myelinated or unmyelinated axons (Fig. 2*D*, *Lower*). Similar results were obtained 21 d after injury (Fig. 2*E* and Fig. S5*A*). Importantly, axon num-

ber, axon width, and axon area distribution profiles in the regenerated distal stump were not significantly different between Sirt2-SCKO and control samples, indicating that axonal regrowth was not impaired in these mutant mice (Fig. 2*F* and Fig. S5 *B* and *C*). The difference in myelin thickness was no longer detectable 28 d postinjury (Fig. 2*E* and Fig. S5*A*). These results show that remyelination after nerve injury, like developmental myelination, is transiently delayed in Sirt2-SCKO mice. Taken together, these data suggest a mechanistic role of Sirt2 in the formation of peripheral myelin.

Par-3 Is a Deacetylation Target of Sirt2. The effects of Sirt2 deficiency on myelin formation prompted us to consider potential deacetylation targets in SCs that might affect this process. Importantly, we did not observe significant changes in the α-tubulin acetylation status in Sirt2-SCKO sciatic nerves (Fig. S6*A*). Furthermore, α-tubulin acetylation was unchanged in a rat SC line overexpressing Sirt2 even when grown in the presence of NAD^+ (Fig. S6*B*). These observations suggest either that α-tubulin is not a major deacetylation target of Sirt2 in SCs or that the acetylation status of α-tubulin following manipulation of Sirt2 can be counterbalanced by other factors in SCs.

To explore additional deacetylation targets that could account for the Sirt2-SCKO phenotype, we next considered molecules with the following properties: (*i*) involved in the regulation of SC myelination, (*ii*) colocalized with Sirt2 in SCs, (*iii*) acetylated, and (*iv*) deacetylated by Sirt2. The polarity protein Par-3 is necessary for normal peripheral myelination (23) and can be detected in SC areas of noncompact myelin with a distribution strikingly similar to that of Sirt2 (24). Indeed, fluorescence immunostaining showed colocalization of Sirt2 and Par-3 in SCs and at regular internodal intervals on teased nerve fibers (Fig. 3*A* and Fig. S6*C*). This result suggests that these proteins colocalize in noncompact myelin in vivo (note that Par-3 also colocalizes with *N*-cadherin at SL incisures) (23, 24). We next examined whether Par-3 was an acetylated protein that could be deacetylated by Sirt2. First, HA-Sirt2 was coexpressed with FLAG-Par-3 in HEK 293T cells and pull-down assays with an anti–FLAG-M2 agarose affinity gel were performed. Indeed, Western blots probed with anti-HA antibodies showed the presence of HA-Sirt2 in the immunoprecipitates, thus demonstrating that these proteins can interact with each other, either directly or indirectly (Fig. 3*B*). Second, to determine whether Sirt2 can deacetylate Par-3, FLAG-Par-3 was immunoprecipitated from cells cotransfected with HA-Sirt2 and Par-3 acetylation was assessed by Western blotting using anti–Acetyl-K antibody. To ensure Par-3 is robustly acetylated we also cotranfected with p300 acetyltransferase because of its reported acetyltransferase activity for nonnuclear substrates (25, 26). This experiment clearly demonstrated that Par-3 is an acetylated protein and that it can be deacetylated by Sirt2 (Fig. 3*C*). Third, FLAG-Par-3 was immunoprecipitated from cells coexpressing p300 acetyltransferase and then incubated with recombinant wild-type or catalytically inactive Sirt2 protein (H150Y substitution) in the presence of NAD^+ with or without nicotinamide (NAM). We found that inhibiting Sirt2 activity genetically or pharmacologically blocked the deacetylation of Par-3 (Fig. 3*D*). These results identify Par-3 as a bona fide Sirt2 deacetylation target and led us to explore the role of Par-3 acetylation in myelin formation.

Sirt2 Regulates aPKC Activation via Par-3 Deacetylation. Par-3, together with Par-6 and aPKC (mammalian isoforms aPKCζ and aPKCι/λ), is a constituent of the Par complex that regulates cell polarity in various species and cell types (27–29). Par-3 interacts with Par-6 and the effector of this complex, aPKC, via distinct domains (27) and thereby controls Par-6 localization and aPKC activation (30, 31). Inhibition of Par complex formation in epithelial cells during development results in delayed morphogenesis via perturbed establishment of apical–basal polarity (32, 33). In premyelinating SCs, Par-3 additionally interacts with $p75^{NTR}$ through its PDZ1 binding domain to relocalize this receptor to axon–glial junctions, thereby promoting in vitro myelination (23). We therefore asked whether Par-3 acetylation status regulated the activity of one or several of these binding partners to, in turn, affect downstream signaling and myelination. We first used tandem mass spectrometry to identify acetylated lysine residues in Par-3. We found four acetylated residues that were regulated by Sirt2 (Lys-831, -848, -881, and -1327) (Fig. 3*E* and Fig. S7), three of which were clustered within the aPKC interaction domain. No acetylated lysines were detected within PDZ1, the domain that interacts with Par-6 and $p75^{NTR}$. Thus, to explore the relationship between Par-3 acetylation and aPKC activation, we examined the phosphorylation state of aPKC using a phospho-specific antibody directed against Thr^{410}, whose phosphorylation is correlated with kinase activation (30, 34). Strikingly, lentivirus-mediated Sirt2 overexpression in rat SCs resulted in decreased Par-3 acetylation and concurrently markedly lower levels of phospho-aPKC (Fig. 3*F*). Moreover, administration of NAD^+ to such SCs, to further stimulate deacetylation by Sirt2, lowered aPKC activation additionally; conversely, treatment with NAM to inhibit Sirt2 activity increased aPKC phosphorylation (Fig. 3*F*). These results indicate that Par-3 acetylation is associated with increased aPKC phosphorylation (i.e., activation) in SCs.

We next studied the relationship between Sirt2 expression, Par-3 acetylation, and aPKC activation in the sciatic nerve in vivo. In accord with our results in cultured SCs, nerves from adult Sirt2-SCKO mice showed hyperacetylation of Par-3 and markedly elevated levels of phospho-aPKC compared with littermate controls (Fig. 3*G*). The abnormal levels of acetylated Par-3 in these mice indicate that other deacetylases cannot compensate for the loss of Sirt2 in vivo and restore Par-3 acetylation status back to normal. To examine whether Par-3 acetylation and aPKC activation are associated with changes during myelination in wild-type animals, Par-3 was immunoprecipitated from lysates of sciatic nerve distal segments, harvested at 7, 14, or 21 d after nerve crush. Consistent with the temporal expression profile of Sirt2, Par-3 acetylation increased substantially by 7 d after crush injury, when remyelination begins and Sirt2 levels are low (Fig. 3*H*). Levels of acetylated Par-3 then declined to normal levels 21 d after injury, when myelination of regenerating fibers is well underway and Sirt2 levels have returned to baseline levels. Remarkably, although phospho-aPKC levels are low in uninjured sciatic nerve, they increase dramatically by day 7 after crush, but then decline as Sirt2 levels increase and Par-3 is deacetylated (Fig. 3*H*). Similar dynamics with decreasing phospho-aPKC levels accompanying increasing Sirt2 expression and decreasing Par-3 acetylation were observed during postnatal myelination (Fig. S8). These data suggest that Sirt2 expression blocks aPKC activation via Par-3 deacetylation in SCs during myelin assembly.

Manipulation of Par-3 Acetylation Status and aPKC Activation Alters Peripheral Myelination. The normal course of myelination correlates with the reciprocal control of Sirt2 expression, Par-3 acetylation, and aPKC activation levels in SCs. These strict temporal relationships suggest that disrupting the dynamic balance between these components by continuous overexpression of Sirt2 could affect myelination. We thus generated transgenic mice in which Sirt2 is overexpressed under control of the constitutive CAGGS promoter selectively in SCs (Sirt2-SCTG) (Fig. 4*A*). At birth, Sirt2 mRNA (Fig. 4*B*) and protein levels were only slightly increased and correspondingly Sirt2-SCTG mice showed no abnormalities in peripheral nerve postnatal development. However, Sirt2 mRNA and protein levels were increased at least approximately twofold in sciatic nerves from adult homozygous Sirt2-SCTG mice (Fig. 4 *B* and *C*). As expected, biochemical analysis in sciatic nerves from adult homozygous Sirt2-SCTG mice demonstrated reduced aPKC phosphorylation (Fig. 4*C*). We thus examined

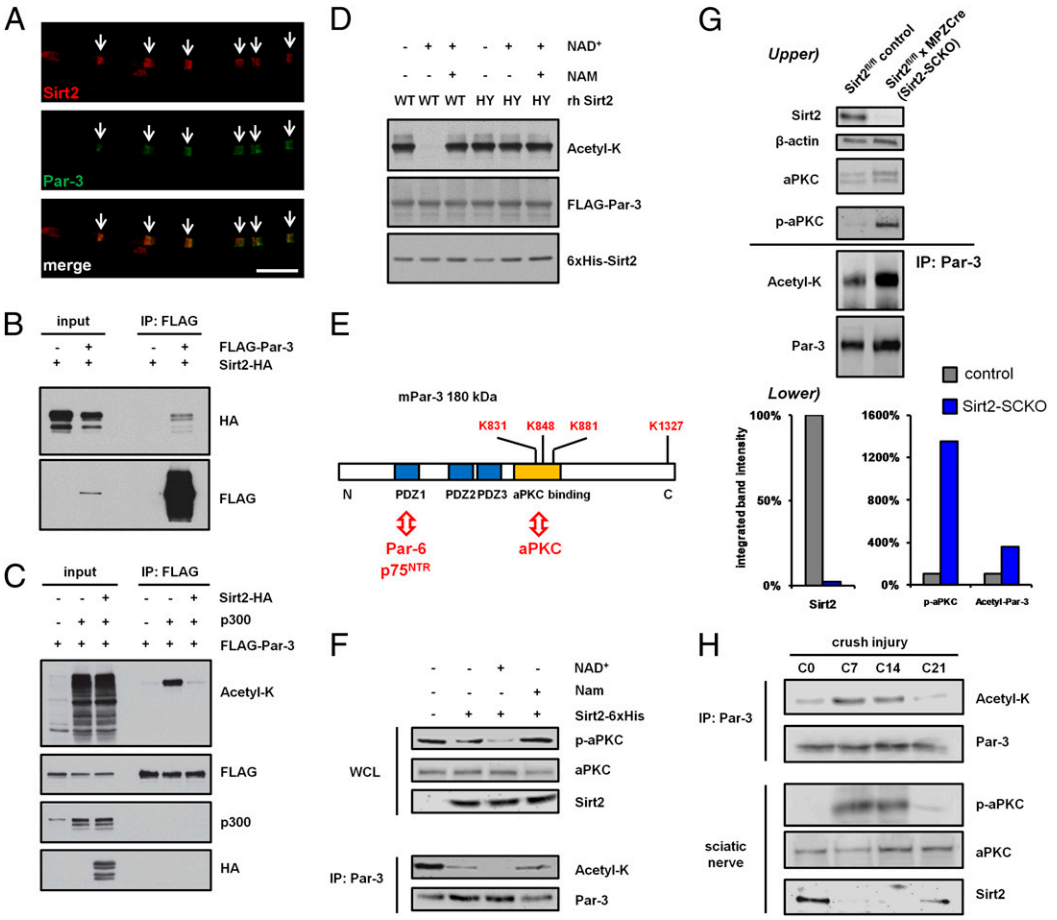

Fig. 3. Sirt2 deacetylates Par-3 and thereby regulates aPKC activation. (*A*) Fluorescence microscopy of rat teased fiber preparation immunolabeled with Sirt2 (red) and Par-3 (green) antibodies. Note colocalization of both signals along internode (indicated by arrows). (Scale bar: 5 μm.) (*B*) Pull-down assay using anti–FLAG-M2 agarose affinity gel and transfected HEK 293T cells overexpressing FLAG-Par-3 or Sirt2-HA or both. Western blots from cell lysates and immunoprecipitates were probed with anti-HA and anti-FLAG antibodies. (*C*) Pull-down assay using anti–FLAG-M2 agarose affinity gel and transfected HEK 293T cells overexpressing Sirt2-HA, p300 acetyltransferase, or FLAG-Par-3 or combinations of these constructs. Western blots from cell lysates and immunoprecipitates were probed with anti–acetyl-lysine, anti-FLAG, anti-p300, and anti-HA antibodies. Note that binding between Sirt2 and Par-3 is not observable in this experiment due to the lower concentration of FLAG-Par-3 in the immunoprecipitate compared with that in *B*. (*D*) Western blots from in vitro Par-3 deacetylation assay using a recombinant human wild-type or point-mutated and therefore deacetylase-deficient Sirt2 (HY) variant. Following Par-3 immunoprecipitation from transfected cells, incubations with recombinant Sirt2 constructs were carried out in the presence of NAD^+, NAM, NAD^+ + NAM, or vehicle control as indicated. The blots were probed with anti–acetyl-lysine, anti-FLAG, and anti-polyhistidine antibodies. (*E*) Schematic illustrating the position of the Sirt2-mediated lysine acetylation sites identified by tandem mass spectrometry relative to individual Par-3 domains responsible for interaction with aPKC, Par-6, and $p75^{NTR}$. (*F*) Western blots from SC lysates and anti-Par-3 immunoprecipitates probed with antibodies against phospho-aPKC, aPKC, Sirt2, acetyl-lysine, and Par-3. SCs were infected with lentivirus for Sirt2 overexpression and were treated with NAD^+ (1 mM), NAM (5 mM), or vehicle beforehand as indicated. WCL: whole-cell lysate. (*G*, *Upper*) Western blots from 2-mo-old Sirt2-SCKO and littermate control sciatic nerve lysates and Par-3 immunoprecipitates probed with antibodies against acetyl-lysine, phospho-aPKC, aPKC, Sirt2, and β-actin (loading control). (*Lower*) Densitometry was used to quantify the intensities of the signals detected above. Sirt2 was normalized to β-actin, phospho-aPKC was normalized to total aPKC, and acetyled Par-3 was normalized to total Par-3 and expressed as percentage of the corresponding signal detected in $Sirt2^{fl/fl}$ control samples. (*H*) Western blots from mouse sciatic nerve lysates and Par-3 immunoprecipates probed with antibodies against acetyl-lysine, phospho-aPKC, aPKC, Sirt2, and Par-3. Sciatic nerve distal stumps were dissected 7, 14, and 21 d following crush lesion and compared with unlesioned nerve preparation (C0).

Sirt2-SCTG mice at 14 d following crush injury and found that remyelination was delayed, as reflected by higher overall *g*-ratios ($P < 0.05$) (Fig. 4*D*) and many axons with considerably thinner myelin sheaths (Fig. 4*F* and Fig. S9*A*). The parameters of axonal regeneration in the distal nerve stump (axon number, axon width, and axon area distribution) were similar to those in control samples (Fig. 4*E* and Fig. S9*B*), indicating that the abnormalities in remyelination are secondary to SC deficits.

To further assess the role of Sirt2 signaling for SC myelination, we used dorsal root ganglion (DRG)/SC cocultures, a valuable model for studying axon–glia interactions during myelin formation (35, 36). Consistent with our in vivo data, Sirt2 knockdown exclusively in SCs by lentivirus-mediated delivery of Sirt2 siRNAs significantly reduced the number of anti–MBP-labeled myelin profiles (Fig. 5 *A* and *B*). In contrast, siRNA-mediated knockdown of Sirt1 in SCs had no appreciable effect on myelination (Fig. 5*B*). Moreover, in accord with results obtained in Sirt2-SCTG mice, Sirt2 overexpression in SCs by lentivirus also reduced myelin formation in vitro (Fig. 5*B*, *Right*).

To directly investigate the role of Par-3 acetylation on myelination, we performed a genetic "add-back" experiment. A Par-3 siRNA construct was developed that effectively knocked down endogenous Par-3 in rat SCs (rPar-3), but did not interfere with expression of mouse Par-3 (mPar-3). Rat SCs were infected with lentivirus expressing rPar-3 siRNA alone or in combination with lentiviruses expressing either wild-type mPar-3 or an mPar-3

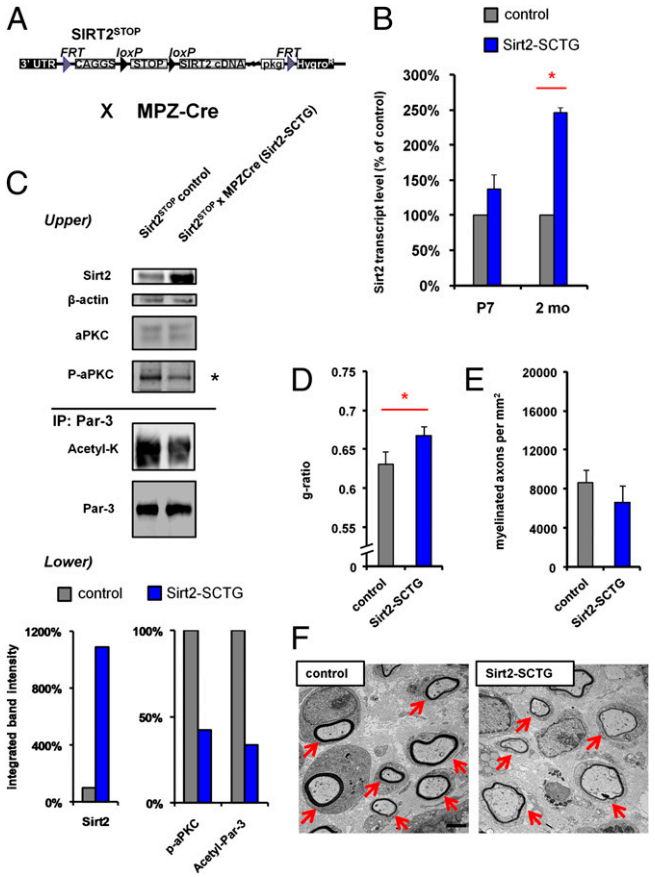

Fig. 4. Characterization of Sirt2-SCTG mice. (*A*) Schematic representation of the Sirt2 transgenic construct that was targeted to the 3′-UTR of the collagen A1 locus of mouse embryonic stem cells by FLP recombination. Transgenic mice carrying this construct were crossed to MPZ-Cre transgenic mice and were bred to homozygosity to generate Sirt2-SCTG mutants and $Sirt2^{STOP}$ controls without Cre recombinase expression. (*B*) qRT-PCR quantification of relative Sirt2 transcript levels (normalized to GAPDH) in sciatic nerves from Sirt2-SCTG transgenics and $Sirt2^{STOP}$ control mice at P7 and 2 mo after birth (n = 3 mice per group tested) (*$P < 0.05$). (*C*, *Upper*) Western blots from 2-mo-old Sirt2-SCTG and littermate control sciatic nerve lysates and Par-3 immunoprecipitates probed with antibodies recognizing Sirt2, β-actin (loading control), phospho-aPKC, aPKC, acetyl-lysine, and Par-3. Note that exposure time at (*) was much longer than in the Western blot shown in Fig. 3*G* to visualize the difference in phospho-aPKC levels in Sirt2-SCTG and littermate control mice. (*Lower*) Densitometry was used to quantify the intensities of the signals detected above. Sirt2 was normalized to β-actin, phospho-aPKC was normalized to total aPKC, and acetyled Par-3 was normalized to total Par-3 and expressed as percentage of the corresponding signal detected in $Sirt2^{STOP}$ control samples. (*D* and *E*) Quantification of *g*-ratios and fiber numbers in distal sciatic nerve stumps 14 d after nerve crush injury in Sirt2-SCTG transgenics and $Sirt2^{STOP}$ control mice (n = 8 mice per group tested) (*$P < 0.05$). (*F*) Transmission electron microscopy of ultrathin sections from distal sciatic nerve stumps 14 d after nerve crush injury in Sirt2-SCTG transgenic and $Sirt2^{STOP}$ control mouse. Arrows point to regenerated fibers. Note thinner compact myelin sheaths around axons from the Sirt2-SCTG preparation. (Scale bar: 2 μm.)

mutant in which the four acetylated lysines were mutated to glutamines to mimic constitutive acetylation [Par-3(4Q)]. When these SCs were used in in vitro myelination assays, we found that myelination was dramatically inhibited by the rPar-3 siRNA. The concomitant expression of mPar-3 substantially restored myelination (~50% of control), whereas the Par-3 acetylation mutant mPar-3(4Q) was inefficient in rescuing this myelination defect (~20% of control) (Fig. 5*C*). These results suggest that Par-3 acetylation status is important for proper myelination.

Finally, we examined the effects of pharmacologically and genetically manipulated aPKC activity on myelination. A peptide inhibitor of aPKCζ (37) was added to the neuron/SC cocultures at the time of induction of the myelination program by ascorbic acid addition or 7 d thereafter when the myelination program is well underway. We found that early inhibition of aPKCζ, before myelin formation started, resulted in a dose-dependent decrease in the number of myelin profiles, but later addition of the aPKC inhibitor did not reduce the number of myelin profiles (Fig. 5*D*). We also examined the impact of aberrantly high aPKC activity by expressing the constitutive active aPKC mutant aPKCζ(T410E) (34) in SCs and then induced myelination in cocultures. We found that high levels of aPKC activity dramatically reduced myelination (Fig. 5*E*). In summary, these experiments suggest that correct temporal control of Sirt2 expression, Par-3 acetylation, and aPKC activation is critical for successful myelin formation.

Discussion

These data demonstrate that Sirt2 dynamically regulates signaling by the polarity complex via the deacetylation of Par-3 in SCs, which in turn alters aPKC activation in a characteristic temporal pattern during developmental myelination and during postinjury remyelination in mice (Fig. 6). The temporal regulation of this pathway is crucial for normal peripheral myelination because ablation or overexpression of Sirt2 and the associated changes in Par-3 acetylation and aPKC activation result in delayed myelin formation.

Sirt2 has been implicated as a modulator of diverse cellular pathways. In view of its suggested role in cell cycle regulation (16), perhaps it is surprising that Sirt2-SCKO mice have normal numbers of SCs in the developing nerve, a time when SCs undergo rapid proliferation (38). This suggests that cell division in SCs is largely independent of Sirt2, an idea supported by the absence of significant alterations in α-tubulin acetylation (which dynamically changes during mitosis) in SCs lacking or overexpressing Sirt2. Indeed, it appears that Sirt2 deacetylates distinct substrates in different cell types. For example, in oligodendrocytes Sirt2 deacetylates α-tubulin, but not histones (39), whereas histone H4 deacetylation is a major Sirt2 activity in other cell types (18). In accord, we unexpectedly discovered that the crucial polarity complex component Par-3 was a robust deacetylation target of Sirt2 in SCs, and this function is important for the myelination deficits caused by aberrant Sirt2 expression. Because Sirt2 is also highly expressed in oligodendrocytes (15), the myelinating glia of the CNS, it will be interesting to determine whether it also regulates Par-3 acetylation and myelin formation in these cells.

The establishment of cell polarity is an important function of SCs, as it is required for their proper alignment with axons and subsequent spiral extension of a vast amount of specialized membrane material to create compact myelin (40). The significance of this function has been demonstrated prominently in DRG/SC cocultures in which knockdown and overexpression of Par-3 resulted in inhibition of myelination (23). On the basis of the identified interaction between Par-3 and the $p75^{NTR}$ receptor (23), this deficit was mechanistically attributed to mislocalization of $p75^{NTR}$ at the axo-glial junction, resulting in failed BDNF signal transduction at this site, which is crucial for myelination. Additionally, the polarity proteins Pals1 and Dlg1 also play a role in myelin assembly in vivo (24, 41). Indeed, many key polarity proteins are expressed in SCs (24), making it increasingly clear that molecular mechanisms used to establish polarity in epithelia are also operant in SCs. Importantly, manipulation of these proteins does not result in global SC dysfunction, but rather in attenuated myelin thickness and in specific defects of myelin formation (24, 41). For example, focal myelin protrusions with similarities to those we observed in Sirt2-SCKO mutants (Fig. S3*C*) are also present in sciatic nerves from mice with down-regulation of the polarity protein Pals1 in SCs (24). With age many of these deficits

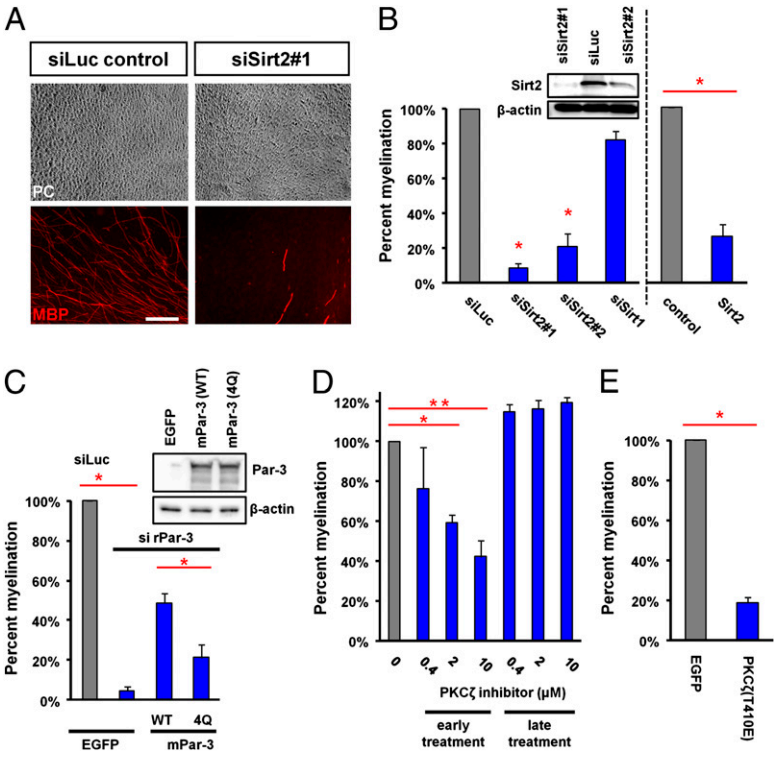

Fig. 5. Manipulation of Sirt2 expression, Par-3 acetylation, and aPKC activation produces myelination abnormalities in DRG/SC cocultures. (*A*) Representative phase-contrast (PC) and fluorescence microscopy from MBP-labeled rat DRG/SC cocultures highlighting myelin profiles on neurites. Before induction of in vitro myelination isolated rat SCs were infected with lentivirus expressing Sirt2 or luciferase (control) siRNA. (Scale bar: 100 μm.) (*B*) Quantification of myelin profiles from in vitro myelination experiments after knockdown of Sirt1 and Sirt2 (*Left*) or overexpression of Sirt2 in SCs (*Right*) (*$P < 0.001$). The results are expressed as percentage of myelination compared with control preparations in which SCs were infected with luciferase siRNA or with empty lentiviral vector (FCIV), respectively. (*Upper*) Knockdown of Sirt2 using two different siRNA target constructs was confirmed by Western blotting. (*C*) Quantification of myelin profiles from in vitro myelination experiments after knockdown of rPar-3 in rat SCs and concomitant expression of mouse Par-3 constructs (wild-type mPar-3 or mutant mPar-3(4Q) mimicking constitutive acetylation). Control preparations were infected with lentivirus for expression of EGFP or luciferase siRNA (*$P <$ 0.01). (*Upper*) Equal expression of the mouse wild-type and mutant Par-3 proteins in the infected SCs was confirmed by Western blotting. (*D*) Quantification of myelin profiles from in vitro myelination experiments after treatment with aPKCζ inhibitor at the induction of myelination by ascorbate addition (early treatment) or 7 d after ascorbate addition (late treatment) (*$P < 0.01$; **$P < 0.005$). (*E*) Quantification of myelin profiles from in vitro myelination experiments after overexpression of constitutive active PKCζ(T410E). Control preparations were infected with lentivirus expressing EGFP (*$P < 0.005$).

in SC polarity mutants become less pronounced (41), also consistent with our results in Sirt2-SCKO mice. In fact, partial to full compensation of hypomyelination occurs in a variety of mouse mutants (e.g., refs. 42 and 43), suggesting the existence of redundant myelination mechanisms.

aPKC signaling regulates cell polarity formation in various cell types (e.g., refs. 28 and 44). Mechanisms by which altered aPKC activation in Sirt2 mutant SCs could affect myelination include the dysregulation of various polarity proteins with their association in complexes (Fig. 6*B*). For example, aPKC phosphorylates Par-3 in a feedback mechanism that can influence its localization; in accord, kinase-dead aPKC causes polarity defects in epithelia via mislocalization of Par-3 (28). These defects occur only in developing cells that are not already fully polarized, a finding consistent with our results demonstrating that early pharmacological inhibition of aPKC affects myelin formation, but not later after myelination is almost completed (Fig. 5*E*). Furthermore, aPKC phosphorylates the polarity proteins Par-1, Lgl, and Crb, the signaling molecule glycogen synthase kinase-3β, and also components regulating the cytoskeleton (45–47). Thus, it will be interesting to determine whether their manipulation in SCs impinges on myelin formation.

Our data together with studies focusing on effects of dietary modulation (9) suggest that SC metabolism could influence myelination via alterations in Sirt2 activity. These results are particularly relevant for diabetic neuropathy where it is believed that reparative responses occur in response to continual nerve damage (48). As sirtuin activity is clearly associated with cellular metabolism, and sirtuin activity is often deregulated in diabetes (49), a role for aberrant Sirt2 activity in impaired SC plasticity during nerve regeneration in diabetes is plausible (5–8, 50). Accordingly, the Sirt2/Par-3/aPKC pathway is a potential therapeutic target for treatment of neuropathy associated with altered metabolic conditions. In this respect, a variety of small molecules targeting sirtuins are already being developed for therapeutic applications in diabetes.

An important question to resolve in future studies is whether Sirt2 in SCs has a neuroprotective role for enhancing the long-term integrity of peripheral nerves. Although adult Sirt2-SCKO mutants showed no morphological or electrophysiological nerve abnormalities, aged animals or those undergoing metabolic stress or repetitive cycles of demyelination and remyelination may show myelin defects. Considering the prominent role of acetylation in metabolic pathways including fatty acid oxidation (51) as well as the relationship between Sirt2 expression and sterol biosynthesis (52), it will be interesting to examine the long-term consequence of Sirt2 loss on myelin lipid composition.

In summary, our data indicate a role for Sirt2 in peripheral myelination with an unexpected link to the regulation of cell polarity in SCs. We discovered that Sirt2 robustly deacetylates Par-3 and thereby dynamically controls activation of aPKC, a crucial signaling component of the polarity complex. We speculate that

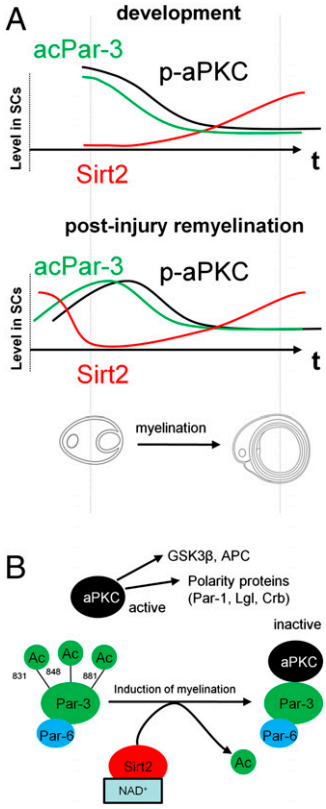

Fig. 6. Molecular modulation of peripheral myelination by the Sirt2/Par-3/aPKC pathway. (*A*) Schematic graphs summarizing the progression of Sirt2 expression, Par-3 acetylation, and phospho-aPKC levels during developmental myelination and remyelination after nerve injury in adult mice. (*B*) Model based on the profiles shown in *A* illustrating how decreases in Par-3 acetylation due to elevated Sirt2 levels result in aPKC inactivation and effects on downstream targets that control myelin assembly in SCs. Such targets include other polarity proteins (e.g., such as Par-1, Lgl, and Crb), signaling molecules, and cytoskeletal regulatory proteins (e.g., GSK3β and APC); see *Discussion* for details.

these findings will improve our understanding of the molecular mechanisms underlying impaired SC plasticity in demyelinating neuropathies with metabolic etiologies. Future studies to explore the therapeutic usefulness of sirtuin manipulation for myelination and nerve repair in such conditions may be rewarding.

Materials and Methods

Quantitative Real-Time PCR. Dissected mouse sciatic nerves were rapidly snap-frozen in liquid nitrogen and homogenized in Ribozol RNA extraction reagent (Amresco). Total RNA was extracted following the manufacturer's protocol and then quantified with an ND-1000 spectrophotometer (Nanodrop Technologies). After reverse transcription using M-MLV reverse transcriptase (Invitrogen) or qScript cDNA SuperMix (Quanta Biosciences), quantitative real-time PCR was carried out using a SYBR green-based assay on an ABI 7700 or 7900 HT sequence detection system (Applied Biosystems) similarly to that described previously (53). Gene expression data from at least three different mice per experimental group were obtained and normalized to glyceraldehyde-3-phosphate dehydrogenase (GAPDH) expression. Primers were as follows: Sirt2 forward, CCATCCACTGGCCTCTATGC; Sirt2 reverse, GGCAGATGGTTGGCTTGAAC; Sirt1 forward, TTGACCGATGGACTCCTCACT; Sirt1 reverse, GATCGGTGCCAATCATGAGA; MPZ forward, CCCTGGCCATTGTGGTTTAC; MPZ reverse, CCATTCACTGGACCAGAAGGAG; GAPDH forward, TGCCCCCATGTTTGTGATG; GAPDH reverse, TGTGGTCATGAGCCCTTCC.

Generation of Conditional Sirt2 Mutant Mice. To generate Sirt2 floxed ($Sirt^{fl/fl}$) mice, genomic DNA covering the *Sirt2* locus was amplified from the 129Sv strain using high-fidelity PCR. The resulting DNA fragments were assembled into the targeting vector that, after linearization by NotI, was electroporated into 129Sv ES cells. G418-resistant colonies were selected and analyzed for homologous recombination by PCR and Southern blot hybridization. For the PCR screening strategy, primers NeoF, 5′-AGGGGCTCGCGCCAGCCGAACTGTT- 3′ and AHR241, 5′-GCGGCCTATATAACTAACGCAGCAG-3′ and primers AHR244, 5′-GATGGAACTCAGCCCCTACACTCAC-3′ and NeoR, 5′-GCGGCCGGAGAACCTGCGTGCAATC-3′ were used. Positive clones were verified by Southern blot hybridization. Ten-kilobase DNA fragments (EcoRV) located from exons 4–7 were used as probes. The karyotype was verified and several correctly targeted ES cell clones were injected into blastocysts from C57BL/6J mice. These blastocysts were transferred into pseudopregnant females, resulting in chimeric offspring that were mated to female C57BL/6J mice that express the Flp recombinase under the control of the ubiquitous CMV promoter. Offspring that transmitted the mutated allele, in which the selection marker was excised and that lost the Flp transgene, were then selected and used for systematic backcrossing with C57BL/6J mice to generate congenic *Sirt2* floxed mouse lines. For Schwann cell-specific Sirt2 ablation starting at early embryonic age, homozygous floxed mice were crossed to MPZ-Cre transgenic mice on a C57BL/6J background (19). To confirm recombination at sites of Cre expression conditional Sirt2 mutants were additionally crossed to ROSA26-YFP reporter mice.

Conditional Sirt2-overexpressing mice were engineered analogous to previously reported Sirt1 transgenics using Flp-mediated genomic integration at the Collagen A1 locus (54). These mice carry a Cre-inducible Sirt2 transgenic construct in which a *loxP* flanked STOP sequence is inserted between the CAGGS promoter and the Sirt2 cDNA (Fig. 4*A*). They were crossed to MPZ-Cre transgenics to generate mice with Sirt2 overexpression specifically in Schwann cells (Sirt2-SCTG).

Genotyping for all mutants was performed by PCR strategies using appropriate primers (sequences available upon request).

Plasmid Constructs. Plasmids were prepared using standard recombinant techniques. For immunoprecipitation and Par-3 deacetylation assays in HEK 293T cells, human Sirt2 was cloned with a C-terminal HA tag sequence into pcDNA3.1(+) vector. P-300 acetyltransferase was cloned into pcDNA3 vector. N-terminal FLAG-Par-3 constructs were a generous gift from J. Fawcett (Dalhousie University, Halifax, NS, Canada). Full-length human Sirt2 cDNA was cloned into pTrcHis vector (Gibco and Invitrogen) for production of recombinant 6xHis-Sirt2. Catalytically inactive H187Y mutant 6xHis-Sirt2 (HY) was generated by a QuikChange Site-Directed Mutagenesis Kit (Stratagene).

For lentiviral-mediated infection of rat SCs, a vector containing the rat Sirt2 cDNA was obtained from OpenBiosystems (7134377; GenBank no. BC086545) and confirmed by DNA sequencing. A 6xHis epitope tag was linked to the C terminus of rat Sirt2 by PCR and the construct subcloned into FCIV, a lentiviral expression vector in which gene expression is driven by the ubiquitin promoter and coexpression of Venus fluorescent protein is enabled by an IRES element (55). For knockdown experiments in rat SCs, oligonucleotides were designed as described previously (56) and lentiviral vectors were constructed by insertion of oligonucleotides containing the respective siRNA target sequences and a hairpin loop into the FSPsi plasmid. In this lentiviral vector the siRNA sequence is driven by the U6 promoter and followed by an SV40 promoter–puromycin resistance cassette to select infected rat SCs. The 19-bp siRNA target sequences were Sirt2 siRNA 1, 5′-GACTCCAAGAAGGCTTACA; Sirt2 siRNA 2, 5′-GGAGCATGCCAACATAGAT; Sirt1 siRNA, TGTTGTTTGTTGCTTGGTC; and Par-3 siRNA, 5′-AAGGATCCAAACTACTGGA.

Luciferase siRNA construct was used as the control. The mouse FLAG-Par-3 constructs in lentiviral expression vector FCIV were generated from a plasmid generously provided by T. Pawson (Samuel Lunenfeld Research Institute, Toronto, ON, Canada) (31). The mouse Par-3(4Q) mutant was produced by site-directed mutagenesis (Stratagene QuikChange). The rat FLAG-PKZζ (T410E) cDNA was purchased from Addgene (10804) and subcloned into the FCIV lentiviral expression vector.

Lentivirus Production. Lentiviruses for infection of SC and Schwannoma cell cultures were produced in HEK 293T cells as described previously (56).

In Vivo Remyelination Assay. All experiments were carried out in accordance with Washington University institutional animal protocols and previously published protocols (22, 57, 58). Adult mice were anesthetized by i.p. injection of avertin. The proximal right sciatic nerves were exposed and crushed at the sciatic notch with an FST no. 5 watchmaker forceps for 30 s, using aseptic surgical conditions. This procedure results in a reproducible compression injury that leads to Wallerian degeneration and subsequently reliable regeneration and remyelination of the distal nerve stump. The crush site was marked with a single 10-0 nylon epineural suture 5 mm proximal and distal to the injury. The muscle layer and skin were reapproximated with

a simple interrupted 4-0 nylon suture. In each mouse, the left sciatic nerve served as the unoperated control sample. After 14, 21, or 28 d the mice were killed and ~15-mm sciatic/tibial nerve segments including the distal regenerated stump were dissected and embedded in epoxy resin. Histomorphometric analysis was carried out 5 mm distal to the crush site on transverse semithin sections stained with toluidine blue as described below.

In Vitro Myelination Assay. In vitro myelination was performed as described previously (59). Briefly, dissociated E15.5 rat DRG neurons were plated onto four-well Nunc plates at 2.5×10^5 cells per well in DMEM–high glucose with 10% FCS, 2 mM L-glutamine, and 50 ng/mL NGF. Glia were eliminated from the cultures by addition of 5-fluoro-2-deoxyuridine (20 μM; Sigma) plus uridine (20 μM; Sigma) to neurobasal medium (Invitrogen) supplemented with B-27 (Invitrogen), 2 mM L-glutamine, 50 ng/mL NGF, and 4 g/L D-glucose for 5 d. Primary rat SC cultures were established from newborn rat sciatic nerves using Brockes' method. SCs were infected with lentivirus and 5 d postinfection cells were positively selected for siRNA expression by growth in 1.5 μg/mL puromycin for 2 d, which was followed by a recovery period of 5 d. For overexpression experiments SCs were infected with lentivirus and Venus fluorescent reporter protein expression was confirmed in almost 100% of cells. The SCs were then plated onto DRG neurons at 200,000 cells per well. Five to 7 d later, in vitro myelination was initiated by switching the medium to F-12/DMEM–high glucose with 15% FCS, 2 mM L-glutamine, 50 ng/mL NGF, and 50 μg/mL ascorbic acid for 14 d. For pharmacological aPKC inhibition experiments, the peptide aPKCζ inhibitor was added to the myelination medium at the indicated concentrations. For visualization of compact myelin, MBP immunostaining was performed as described previously after the cultures have been allowed to myelinate for 14 d (59). Quantification of the efficiency to initiate myelin formation was calculated by counting the number of MBP-positive internodes in five fields at 200× magnification and setting the control to 100%. Each condition was performed in quadruplicate wells, and the data for each experiment shown are the average of three independent experiments (mean ± SEM).

Preparation of Protein Lysates, Immunoprecipitations, and Western Blotting. Sciatic nerves were rapidly dissected and immediately frozen in liquid nitrogen. Nerve lysates were prepared by homogenizing the tissue with a sonicator in RIPA buffer (50 mM Tris, pH 7.5, 150 mM NaCl, 1% Triton, 1% Nonidet P-40, 1% deoxycholate, 0.1% SDS, 10 mM EDTA, 10 mM sodium fluoride, and 1 mM sodium vanadate) or a buffer containing 2% SDS, 10% glycerol, 1 mM sodium vanadate, 1 mM β-glycerophosphate, and 1 mM PMSF in TBS. Both buffers were supplemented with Complete Protease Inhibitor Mixture (Roche). For cultured cells, lysis was performed by sonication in IP buffer [10 mM Tris, pH 7.4, 1% Triton X-100, 0.5% Nonidet P-40, 150 mM NaCl, and Complete Protease Inhibitor Mixture (Roche)]. For preservation of immunoprecipitated Par-3 acetylation the lysis buffers were supplemented with 10 mM nicotinamide and 100 nM trichostatin A. The lysates were clarified by centrifugation and protein concentrations in the supernatants were measured using the Micro BCA protein assay kit (Thermo Scientific). For the individual immunoprecipitation experiments, the lysates were incubated with the indicated antibodies and Protein-G Agarose beads (rProtein G; Invitrogen) for 2 h or overnight at 4 °C or anti–FLAG-M2 agarose affinity gel for o/n at 4 °C. The precipitated proteins bound to Agarose beads were then repeatedly washed by centrifugation and the final pellets diluted in Laemmli buffer. For Western blotting, proteins were separated by SDS/PAGE according to standard protocols and blotted to nitrocellulose or PVDF membranes using wet transfer (Bio-Rad). After blocking and incubation with the indicated primary antibodies (o/n) and HRP-coupled secondary antibodies (1 h), protein bands were visualized using SuperSignal West Dura substrate (Pierce) and the UVP Bioimaging System (Epi Chemi II Darkroom).

In Vitro Par-3 Deacetylation Assay. DH5α bacteria (Invitrogen) were transformed with pTrcHis-Sirt2 or pTrcHis-Sirt2 (HY), grown at 37 °C, induced with 0.1 mM isopropyl-β-D-thiogalactopyranoside (IPTG) at an OD_{A600}, and grown for an additional 2 h. The resulting 6× His-tagged proteins were purified as described previously (60) and recombinant proteins were aliquoted and stored at −20 °C. FLAG-Par-3 was coexpressed with p300 acetyltransferase in HEK 293T cells and immunoprecipitated as described above. Immunoprecipitated FLAG-Par-3 was then washed for an additional 15 min in Sirt2 deacetylase buffer (50 mM Tris·HCl, pH 9.0, 4 mM MgCl2, and 0.2 mM DTT). Both immunoprecipitated material and recombinant Sirt2 variants were resuspended in 50 μL of Sirt2 deacetylase buffer with and without nicotinamide. The enzymatic reactions were started by addition of NAD^+, incubated for 2 h at 30 °C, and stopped by adding 10 μL 6× Laemmli buffer with β-mercaptoethanol. The acetylation status of Par-3 was assessed by Western blotting, applying anti–acetyl-lysine antibody.

Mapping of Acetylation Sites by LC-MS/MS. Material from in vitro Par-3 deacetylation assays was separated by SDS/PAGE and stained with Coomassie Brilliant Blue (Bio-Rad). Bands corresponding to Par-3 were cut and washed thoroughly in water followed by three washes with 50% acetonitrile. The excised gel bands were sent to the Taplin mass spectrometry core (Harvard Medical School) where they were cut into ~1-mm^3 pieces. The samples were reduced with 1 mM DTT for 30 min at 60 °C and then alkylated with 5 mM iodoacetamide for 15 min in the dark at room temperature. Gel pieces were then subjected to a modified in-gel trypsin digestion procedure (61). Gel pieces were washed and dehydrated with acetonitrile for 10 min followed by removal of acetonitrile. Pieces were then completely dried in a speed-vac. Rehydration of the gel pieces was performed with 50 mM ammonium bicarbonate solution containing 12.5 ng/μL modified sequencing-grade trypsin (Promega) at 4 °C. Samples were then placed in a 37 °C room overnight. Peptides were later extracted by removing the ammonium bicarbonate solution, followed by one wash with a solution containing 50% acetonitrile and 5% acetic acid. The extracts were then dried in a speed-vac (~1 h) and stored at 4 °C until analysis.

On the day of analysis the samples were reconstituted in 5 μL of HPLC solvent A (2.5% acetonitrile, 0.1% formic acid). A nanoscale reverse-phase HPLC capillary column was created by packing 5-μm C18 spherical silica beads into a fused silica capillary (100 μm inner diameter × 12 cm length) with a flame-drawn tip. After equilibrating the column each sample was pressure loaded off-line onto the column. The column was then reattached to the HPLC system. A gradient was formed and peptides were eluted with increasing concentrations of solvent B (97.5% acetonitrile, 0.1% formic acid). As each peptide was eluted they were subjected to electrospray ionization and then they entered into an LTQ-Orbitrap mass spectrometer (ThermoFinnigan). Eluting peptides were detected, isolated, and fragmented to produce a tandem mass spectrum of specific fragment ions for each peptide. Peptide sequences (and hence protein identity) were determined by matching protein or translated nucleotide databases with the acquired fragmentation pattern by the software program, Sequest (ThermoFinnigan). The modification of 42.0106 mass units to lysine was included in the database searches to determine acetylated peptides. Each acetylated peptide that was determined by the Sequest program was also manually inspected to ensure confidence.

Microscopic Imaging and Histomorphometry. A Nikon Eclipse 80i microscope system coupled to a digital camera (CoolSnapES; Photometrics) was used for presentation of brightfield and epifluorescence images of plastic semithin sections and teased fibers. Images were processed using Metamorph (Version 6.2r4) and global adjustments in brightness and contrast were carried out with Adobe Photoshop. For histomorphometric analysis of nerve structure parameters (*g*-ratio, fiber/axon numbers, axon width, and axon area distribution) in sciatic nerve segments, analysis was carried out as previously described (22) using an automated digital imaging analysis system and custom-made morphometry software (Leco IA32; Leco Instruments). Confocal imaging was performed using a Zeiss LSM5 Pascal confocal system and Zeiss Confocal Software (Version 3.2 SP2). A multitrack configuration mode was applied to avoid crosstalk between individual fluorophores.

Statistical Analysis. All statistical analyses were performed using Microsoft Excel. All data are presented as mean ± SEM. A two-tailed Student's test was used for group comparisons and statistical significance was considered if $P < 0.05$.

For further experimental procedures see *SI Materials and Methods*.

ACKNOWLEDGMENTS. We are grateful to Nina Panchenko and Lauren Cronk for technical assistance with mouse breeding, Timothy Fahrner for help with immunoprecipitations, Daniel Hunter for providing helpful technical advice on nerve morphometry, Josiah Gerdts for help with data illustration, Dr. Elisabetta Babetto for critical reading of the manuscript, and members of the J.M. laboratory for helpful discussions. We acknowledge Drs. Lawrence Wrabetz and Albee Messing for providing MPZCre transgenic mice, Drs. J. Fawcett (Department of Pharmacology, Dalhousie University) and T. Pawson (Samuel Lunenfeld Research Institute, Mount Sinai Hospital) for Par-3 constructs, and Dr. M. Tainsky (Wayne State University) for providing Sirt2 antibodies. This work was supported by National Institutes of Health Neuroscience Blueprint Center Core Grant P30 NS057105 to Washington University; the Hope Center for Neurological Disorders; National Institutes of Health Grants NS040745 and AG13730 (to J.M.), DK59820 (to J.A.), AG027916 and AG028730 (to D.A.S.), DK19645 (to R.E.S.), NS055980 (to R.H.B.), and R21NS059566 (to J.P.G.); Fondation Recherche Médicale (H.Y.); Swiss National Science Foundation Grant

31003A-124713/1 (to J.A.); European Research Council Grant 2008-AdG-23118 (to J.A.); Ellison Medical Foundation (D.A.S.); and Glenn Medical Foundation (D.A.S.). B.B. held a European Molecular Biology Organization long-term fellowship during conduction of the study.

1. Nave KA (2010) Myelination and support of axonal integrity by glia. *Nature* 468: 244–252.
2. Fawcett JW, Keynes RJ (1990) Peripheral nerve regeneration. *Annu Rev Neurosci* 13: 43–60.
3. Jessen KR, Mirsky R (2010) Control of Schwann cell myelination. *F1000 Biol Rep* 2:19.
4. Le N, et al. (2005) Nab proteins are essential for peripheral nervous system myelination. *Nat Neurosci* 8:932–940.
5. Ekström AR, Tomlinson DR (1989) Impaired nerve regeneration in streptozotocin-diabetic rats. Effects of treatment with an aldose reductase inhibitor. *J Neurol Sci* 93: 231–237.
6. Kennedy JM, Zochodne DW (2005) Impaired peripheral nerve regeneration in diabetes mellitus. *J Peripher Nerv Syst* 10:144–157.
7. Sharma AK, Thomas PK (1975) Peripheral nerve regeneration in experimental diabetes. *J Neurol Sci* 24:417–424.
8. Apfel SC (1999) Nerve regeneration in diabetic neuropathy. *Diabetes Obes Metab* 1: 3–11.
9. Madorsky I, et al. (2009) Intermittent fasting alleviates the neuropathic phenotype in a mouse model of Charcot-Marie-Tooth disease. *Neurobiol Dis* 34:146–154.
10. Rangaraju S, et al. (2009) Molecular architecture of myelinated peripheral nerves is supported by calorie restriction with aging. *Aging Cell* 8:178–191.
11. Nagarajan R, Le N, Mahoney H, Araki T, Milbrandt J (2002) Deciphering peripheral nerve myelination by using Schwann cell expression profiling. *Proc Natl Acad Sci USA* 99:8998–9003.
12. Yamamoto H, Schoonjans K, Auwerx J (2007) Sirtuin functions in health and disease. *Mol Endocrinol* 21:1745–1755.
13. Haigis MC, Sinclair DA (2010) Mammalian sirtuins: Biological insights and disease relevance. *Annu Rev Pathol* 5:253–295.
14. North BJ, Marshall BL, Borra MT, Denu JM, Verdin E (2003) The human Sir2 ortholog, SIRT2, is an NAD+-dependent tubulin deacetylase. *Mol Cell* 11:437–444.
15. Li W, et al. (2007) Sirtuin 2, a mammalian homolog of yeast silent information regulator-2 longevity regulator, is an oligodendroglial protein that decelerates cell differentiation through deacetylating alpha-tubulin. *J Neurosci* 27:2606–2616.
16. Dryden SC, Nahhas FA, Nowak JE, Goustin AS, Tainsky MA (2003) Role for human SIRT2 NAD-dependent deacetylase activity in control of mitotic exit in the cell cycle. *Mol Cell Biol* 23:3173–3185.
17. Jing E, Gesta S, Kahn CR (2007) SIRT2 regulates adipocyte differentiation through FoxO1 acetylation/deacetylation. *Cell Metab* 6:105–114.
18. Vaquero A, et al. (2006) SirT2 is a histone deacetylase with preference for histone H4 Lys 16 during mitosis. *Genes Dev* 20:1256–1261.
19. Feltri ML, et al. (1999) P0-Cre transgenic mice for inactivation of adhesion molecules in Schwann cells. *Ann N Y Acad Sci* 883:116–123.
20. Gonçalves AF, et al. (2010) Gelsolin is required for macrophage recruitment during remyelination of the peripheral nervous system. *Glia* 58:706–715.
21. Song XY, Zhou FH, Zhong JH, Wu LL, Zhou XF (2006) Knockout of p75(NTR) impairs re-myelination of injured sciatic nerve in mice. *J Neurochem* 96:833–842.
22. Hunter DA, et al. (2007) Binary imaging analysis for comprehensive quantitative histomorphometry of peripheral nerve. *J Neurosci Methods* 166:116–124.
23. Chan JR, et al. (2006) The polarity protein Par-3 directly interacts with p75NTR to regulate myelination. *Science* 314:832–836.
24. Ozçelik M, et al. (2010) Pals1 is a major regulator of the epithelial-like polarization and the extension of the myelin sheath in peripheral nerves. *J Neurosci* 30:4120–4131.
25. Jiang W, et al. (2011) Acetylation regulates gluconeogenesis by promoting PEPCK1 degradation via recruiting the UBR5 ubiquitin ligase. *Mol Cell* 43:33–44.
26. Zhao Y, et al. (2010) Cytosolic FoxO1 is essential for the induction of autophagy and tumour suppressor activity. *Nat Cell Biol* 12:665–675.
27. Joberty G, Petersen C, Gao L, Macara IG (2000) The cell-polarity protein Par6 links Par3 and atypical protein kinase C to Cdc42. *Nat Cell Biol* 2:531–539.
28. Ohno S (2001) Intercellular junctions and cellular polarity: The PAR-aPKC complex, a conserved core cassette playing fundamental roles in cell polarity. *Curr Opin Cell Biol* 13:641–648.
29. Macara IG (2004) Parsing the polarity code. *Nat Rev Mol Cell Biol* 5:220–231.
30. Hirai T, Chida K (2003) Protein kinase Czeta (PKCzeta): Activation mechanisms and cellular functions. *J Biochem* 133:1–7.
31. Lin D, et al. (2000) A mammalian PAR-3-PAR-6 complex implicated in Cdc42/Rac1 and aPKC signalling and cell polarity. *Nat Cell Biol* 2:540–547.
32. Etienne-Manneville S, Hall A (2003) Cell polarity: Par6, aPKC and cytoskeletal crosstalk. *Curr Opin Cell Biol* 15:67–72.
33. Horikoshi Y, et al. (2009) Interaction between PAR-3 and the aPKC-PAR-6 complex is indispensable for apical domain development of epithelial cells. *J Cell Sci* 122: 1595–1606.
34. Chou MM, et al. (1998) Regulation of protein kinase C zeta by PI 3-kinase and PDK-1. *Curr Biol* 8:1069–1077.
35. Wood P, et al. (1990) Studies of the initiation of myelination by Schwann cells. *Ann N Y Acad Sci* 605:1–14.
36. Jessen KR, Mirsky R (1991) Schwann cell precursors and their development. *Glia* 4: 185–194.
37. Vohra BP, Fu M, Heuckeroth RO (2007) Protein kinase Czeta and glycogen synthase kinase-3beta control neuronal polarity in developing rodent enteric neurons, whereas SMAD specific E3 ubiquitin protein ligase 1 promotes neurite growth but does not influence polarity. *J Neurosci* 27:9458–9468.
38. Jessen KR, Mirsky R (2005) The origin and development of glial cells in peripheral nerves. *Nat Rev Neurosci* 6:671–682.
39. Harting K, Knöll B (2010) SIRT2-mediated protein deacetylation: An emerging key regulator in brain physiology and pathology. *Eur J Cell Biol* 89:262–269.
40. Etienne-Manneville S (2008) Polarity proteins in glial cell functions. *Curr Opin Neurobiol* 18:488–494.
41. Cotter L, et al. (2010) Dlg1-PTEN interaction regulates myelin thickness to prevent damaging peripheral nerve overmyelination. *Science* 328:1415–1418.
42. Giacomini C, et al. (2011) Both Schwann cell and axonal defects cause motor peripheral neuropathy in Ebf2-/- mice. *Neurobiol Dis* 42:73–84.
43. Jaegle M, et al. (1996) The POU factor Oct-6 and Schwann cell differentiation. *Science* 273:507–510.
44. Tanabe K, et al. (2010) Atypical protein kinase C regulates primary dendrite specification of cerebellar Purkinje cells by localizing Golgi apparatus. *J Neurosci* 30: 16983–16992.
45. Suzuki A, Ohno S (2006) The PAR-aPKC system: Lessons in polarity. *J Cell Sci* 119: 979–987.
46. Etienne-Manneville S, Hall A (2003) Cdc42 regulates GSK-3beta and adenomatous polyposis coli to control cell polarity. *Nature* 421:753–756.
47. Chen YM, et al. (2006) Microtubule affinity-regulating kinase 2 functions downstream of the PAR-3/PAR-6/atypical PKC complex in regulating hippocampal neuronal polarity. *Proc Natl Acad Sci USA* 103:8534–8539.
48. Mizisin AP, et al. (2007) Comparable myelinated nerve pathology in feline and human diabetes mellitus. *Acta Neuropathol* 113:431–442.
49. Imai S, Guarente L (2010) Ten years of NAD-dependent SIR2 family deacetylases: Implications for metabolic diseases. *Trends Pharmacol Sci* 31:212–220.
50. Zochodne DW (2007) Diabetes mellitus and the peripheral nervous system: Manifestations and mechanisms. *Muscle Nerve* 36:144–166.
51. Zhao S, et al. (2010) Regulation of cellular metabolism by protein lysine acetylation. *Science* 327:1000–1004.
52. Luthi-Carter R, et al. (2010) SIRT2 inhibition achieves neuroprotection by decreasing sterol biosynthesis. *Proc Natl Acad Sci USA* 107:7927–7932.
53. Nagarajan R, et al. (2001) EGR2 mutations in inherited neuropathies dominant-negatively inhibit myelin gene expression. *Neuron* 30:355–368.
54. Firestein R, et al. (2008) The SIRT1 deacetylase suppresses intestinal tumorigenesis and colon cancer growth. *PLoS ONE* 3:e2020.
55. Araki T, Sasaki Y, Milbrandt J (2004) Increased nuclear NAD biosynthesis and SIRT1 activation prevent axonal degeneration. *Science* 305:1010–1013.
56. Gustin JA, Yang M, Johnson EM, Jr., Milbrandt J (2007) Deciphering adaptor specificity in GFL-dependent RET-mediated proliferation and neurite outgrowth. *J Neurochem* 102:1184–1194.
57. Lee M, Doolabh VB, Mackinnon SE, Jost S (2000) FK506 promotes functional recovery in crushed rat sciatic nerve. *Muscle Nerve* 23:633–640.
58. Magill CK, et al. (2010) The differential effects of pathway- versus target-derived glial cell line-derived neurotrophic factor on peripheral nerve regeneration. *J Neurosurg* 113:102–109.
59. Ryu EJ, et al. (2008) Analysis of peripheral nerve expression profiles identifies a novel myelin glycoprotein, MP11. *J Neurosci* 28:7563–7573.
60. North BJ, Schwer B, Ahuja N, Marshall B, Verdin E (2005) Preparation of enzymatically active recombinant class III protein deacetylases. *Methods* 36:338–345.
61. Shevchenko A, et al. (1996) Linking genome and proteome by mass spectrometry: Large-scale identification of yeast proteins from two dimensional gels. *Proc Natl Acad Sci USA* 93:14440–14445.